Sensors and Materials, Vol. 35, No. 2 (2023) 537–544
MYU Tokyo

S & M 3192

Development of a Bragg-edge Neutron Transmission Imaging Detector Combined with Micro-structured Boron Cathode and Glass Gas Electron Multiplier

Takeshi Fujiwara,[1,2*] Koichi Kino,[1,2] Nagayasu Oshima,[1,2] and Michihiro Furusaka[1,2]

[1]National Institute of Advanced Industrial Science and Technology (AIST),
1-1-1 Umezono, Tsukuba, Ibaraki 305-8568, Japan
[2]Innovative Structural Materials Association (ISMA),
10th Sanshi-kaikan, 1-9-4 Yurakucho, Chiyoda, Tokyo 100-0006, Japan

(Received October 18, 2022; accepted January 12, 2023)

Keywords: neutron detector, Bragg edge imaging, GEM, glass GEM, AISTANS

A neutron detector with a micro-structured boron cathode and a glass gas electron multiplier (GEM) has been developed for time-of-flight Bragg edge neutron transmission imaging. The detector has a field of view of 100 × 100 mm^2 and 128 × 128 pixels (pixel size 0.8 × 0.8 mm^2). The neutron imaging performance of the detector was evaluated at a compact electron accelerator-driven neutron source (AISTANS). By comparison with a Li-glass detector, we found that our detector has a detection efficiency of 5% for 4 Å neutrons. In addition, a preliminary time-of-flight neutron imaging test was performed to observe the difference between the face-centered and body-centered cubic crystal structures, from which we confirmed that our detector has sufficient stability and time resolution for use in Bragg edge imaging analysis.

1. Introduction

Since the first neutron time-of-flight (TOF) measurement was carried out in the 1960s, the neutron TOF has played an important role in material science.[1,2] Decades after this first measurement, the Bragg edge neutron transmission method has been established as a new analysis technique that can map the microstructural information of materials over a wide area with the advent of pulsed neutron sources such as SNS, ISIS, and J-PARC.[3–6] In recent years, with the development of compact accelerator-driven neutron source technology and the technology of moderators and targets, it has become possible to obtain data of sufficient quality in the wavelength band useful for Bragg edge neutron imaging at small facilities.[7–11] On the other hand, for Bragg edge imaging, a 2D detector with timing information is required. Moreover, the detectors must have sufficient field of view, spatial resolution, uniformity, neutron detection efficiency, long-term stability, low γ-ray sensitivity, and high counting rate capability. Various types of neutron detectors such as scintillation, gas electron multiplier (GEM)-based,

*Corresponding author: e-mail: fujiwara-t@aist.go.jp
https://doi.org/10.18494/SAM4147

ISSN 0914-4935
https://myukk.org/

micro-pixel chamber (μ-PIC), and micro-channel plate (MCP) detectors have been reported.[12–17]

On the other hand, we are developing a detector based on a glass GEM to meet the specifications required for Bragg edge imaging with a simpler structure. Glass GEMs are detectors that use glass as a substrate, whereas conventional GEMs use a thin polyimide foil as an insulator.[18,19] In contrast to foils, glass substrates are rigid and have greater tolerance against discharges. In addition, since glass is chemically stable, long-time stability can be expected. Also, glass GEMs have the advantage of high gas gain capability due to their long gas amplification range compared with conventional GEMs. Therefore, a single glass GEM can provide a sufficient gas gain (~1000), whereas conventional GEMs must be cascaded. Furthermore, whereas conventional boron gas detectors have complicated structures such as stacked boron-coated GEMs, we are developing a micro-structured boron cathode to obtain a high detection efficiency without degrading the spatial resolution while using a simpler detector setup. In this study, a new GEM-based detector with a glass GEM and a micro-structured boron cathode was developed to achieve sufficient performance for Bragg-edge neutron transmission imaging while simplifying the detector structure and making it easier to handle. Here, we outline the basic design of the detector and present the results of Bragg edge neutron transmission imaging at AISTANS, which is a newly developed compact electron accelerator-driven pulsed neutron facility in National Institute of Advanced Industrial Science and Technology (AIST).

2. Materials and Methods

2.1 General design of detector

Figure 1 shows the general design of our time-resolving neutron detector. The detector consists of a GEM (see Sect. 2.2), a boron cathode (see Sect. 2.3), and readout pads and is installed in a gas-filled chamber. The nuclear reaction of a neutron with ^{10}B produces charged particles (alpha particle and ^{7}Li nucleus). Each particle escapes from the boron layer and deposits its energy in the gas volume, causing ionization. Here, Ar/CO_2 (90:10, 1 bar), which is hydrogen-free and readily available, is used as the detector gas medium. The primary electrons generated by this charged particle are multiplied by the glass GEM and then read out via 0.8-mm-pitch readout pads. The readout pads are connected to 128 strips for each axis to achieve a 2D position readout. These signals are processed by application-specific integrated circuits (ASICs) and a field-programmable gate array (FPGA)-based data acquisition board, and the digitized time-resolved neutron data are transferred to a PC via Ethernet (BBTX-067, Bee Beans Technology Co., Ltd.).

2.2 Glass GEM

The glass GEM uses a glass substrate instead of a thin polyimide foil.[19,20] There are 128269 holes in the 100 × 100 mm^2 glass GEM, and each hole acts as a proportional counter, enabling

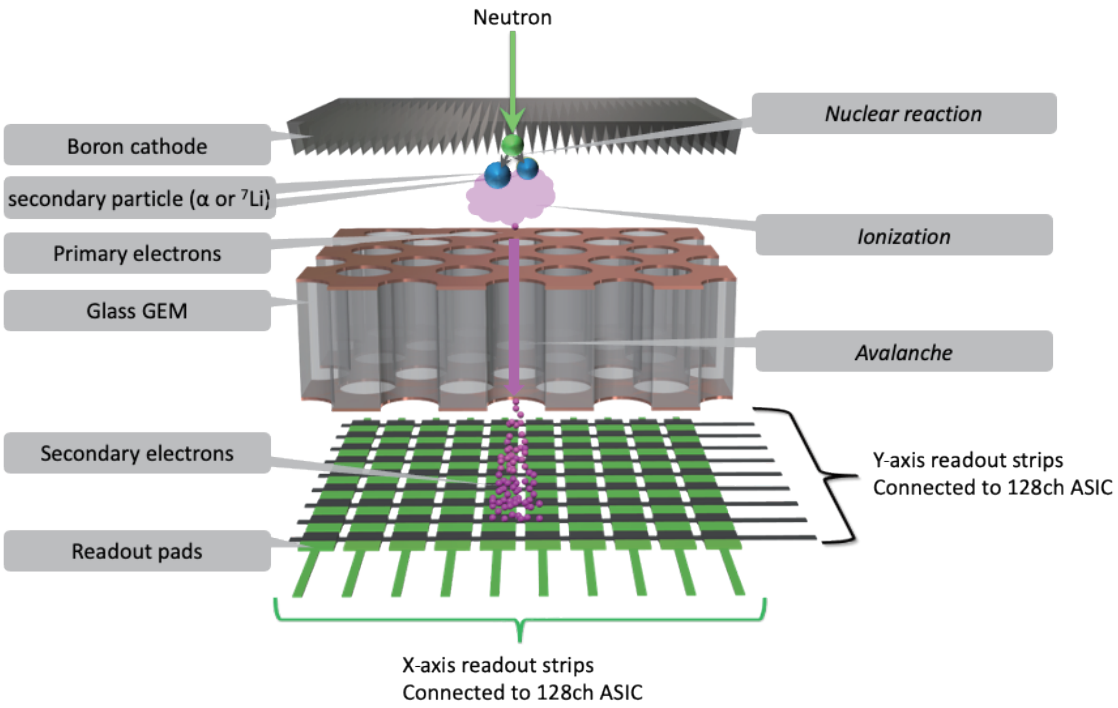

Fig. 1. (Color online) General design of the time-resolving, 2D neutron detector (not to scale).

the signals to be amplified two-dimensionally with a high spatial resolution. To obtain the same electron avalanche amplification at every readout pixel, it is desirable to have a uniform electric field for electron acceleration within every hole. If the sheet curvature changes, the electric field strength distribution will also change nonuniformly, and, as a result, the amplification performance of the GEM may also change. For Bragg edge imaging, it is necessary to collect a sufficient amount of statistical data, which inevitably leads to long measurement times. Furthermore, it may take several months to a year for multiple measurements. For this reason, a rigid glass substrate is used instead of a conventional GEM (which is made of a flexible polyimide thin film), so that the curvature does not easily change.

A photograph of the glass GEM is shown in Fig. 2(a). The hole diameter, hole pitch, and thickness of the glass substrate of the glass GEM used in this study are 190, 280, and 550 μm, respectively. Cu electrodes are metallized on both sides of the hole-drilled glass substrate. Here, we optimized the Cu metallization process, and, as shown in Figs. 2(b) and 2(c), the edges of the electrode are smoother than those in our past works.[20,21] Consequently, the rate of discharge significantly decreased during the operation of the glass GEM. Because of the high gas gain capability of glass GEMs, a single glass GEM can provide a sufficient gas gain of ~1000, while conventional GEMs must be cascaded to achieve a sufficient gas gain. This simplifies the structure of the detector and facilitates maintenance. In addition, owing to the rigidity of the glass substrate, the glass GEM can be easily installed in a gas chamber. In addition, since the volume resistance of the glass substrate is relatively low (polyimide = 1×10^{18} Ω·cm, glass = 8.5×10^{12} Ω·cm), the detector can be operated without charge-up at practical beam intensities.

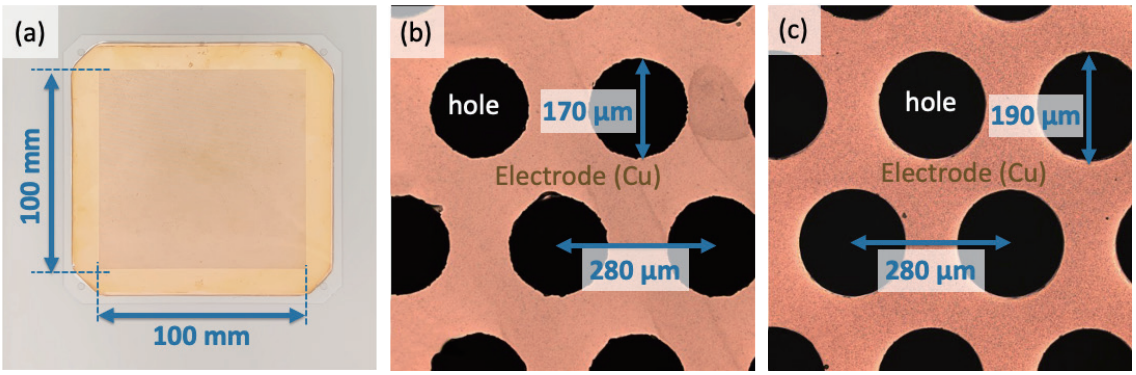

Fig. 2. (Color online) (a) Photograph of the glass GEM. (b) Micrograph of the glass GEM fabricated in past work. (c) Micrograph of the optimized glass GEM.

2.3 Boron cathode

Detection efficiency is another important factor for neutron detectors. We chose ^{10}B for the material for the neutron converter because it has a large cross section for neutrons and is readily available commercially. However, achieving a high neutron detection efficiency is not simple. For neutron detection, a secondary particle from the ^{10}B layer generated by the nuclear reaction must exit the ^{10}B convertor and deposit its energy in the gas medium. Since the track of secondary particles in the ^{10}B layer is 1 to 2 µm, thickening the ^{10}B layer does not improve the detection efficiency because the particles will be absorbed in the layer (the particles will not reach the gas medium). Here, aiming to achieve a higher detection efficiency, we fabricated a micro-structured boron converter for the neutron converter. Instead of using a flat boron substate, a 1-mm-thick aluminum substrate was processed with a sharp blade to create 200-µm-depth canyons over the entire 100 × 100 mm^2 area of the substrate [Figs. 3(a) and 3(b)]. These tiny aluminum canyons were formed with a 150 µm pitch. Finally, a 2-µm-thick ^{10}B layer was deposited on the aluminum substrate. Figure 3(c) shows a cross-sectional view of the structural design of the neutron converter. As a result of its use, the effective thickness of the ^{10}B layer against the neutron beam is expected to increase, and the flight path of the secondary particles generated by the nuclear reaction in the converter layer is expected to decrease [Fig. 3(d)].

3. Experimental Results and Discussion

The neutron imaging test was carried out at AISTANS.[10,11] The electron beam power in this test was 1 kW. Figure 4(a) shows the neutron transmission image of a Cd plate and neutron radiograph indicators produced by American Society for Testing and Materials (ASTM), obtained with this detector.[22] This figure was reconstructed without using TOF information and is therefore a transmission image integrated over the entire neutron wavelength range. The area where neutrons have been absorbed by Cd pieces appears clearly in the neutron transmission image. Figure 4(b) shows the edge fitting result obtained using the error function method.[23]

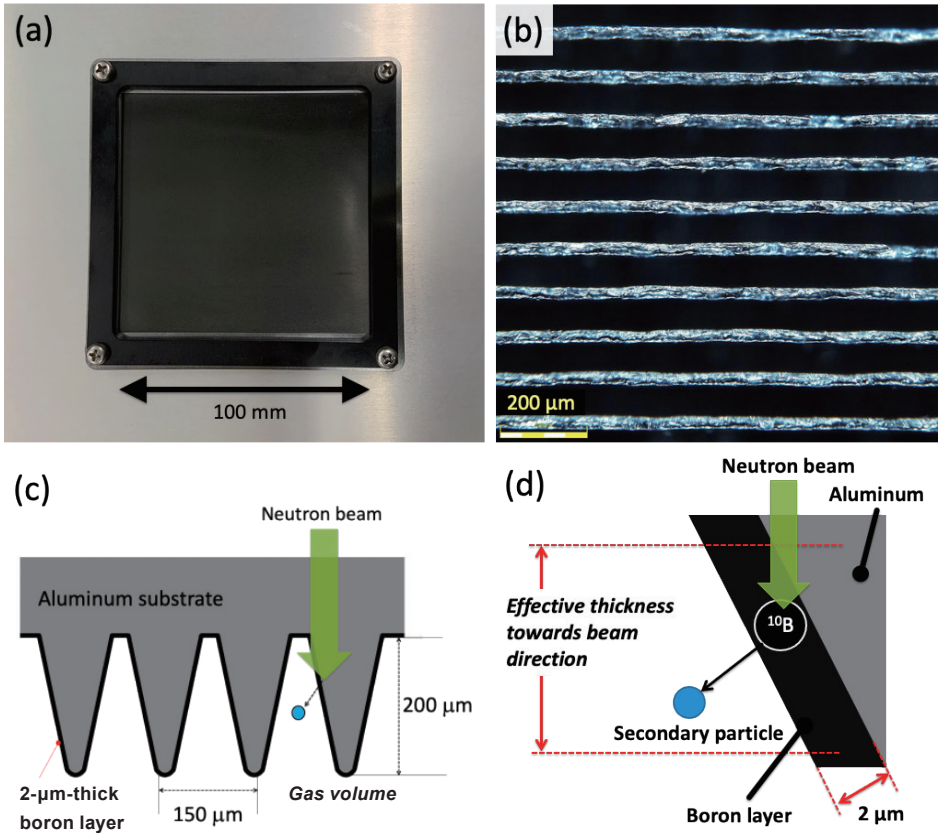

Fig. 3. (Color online) (a) Photograph and (b) micrograph of the micro-structured boron cathode viewed from the glass GEM side. (c) Cross-sectional view of the design of the micro-structured boron cathode. (d) Enlarged cross-sectional view of the cathode, explaining the concept of the structure.

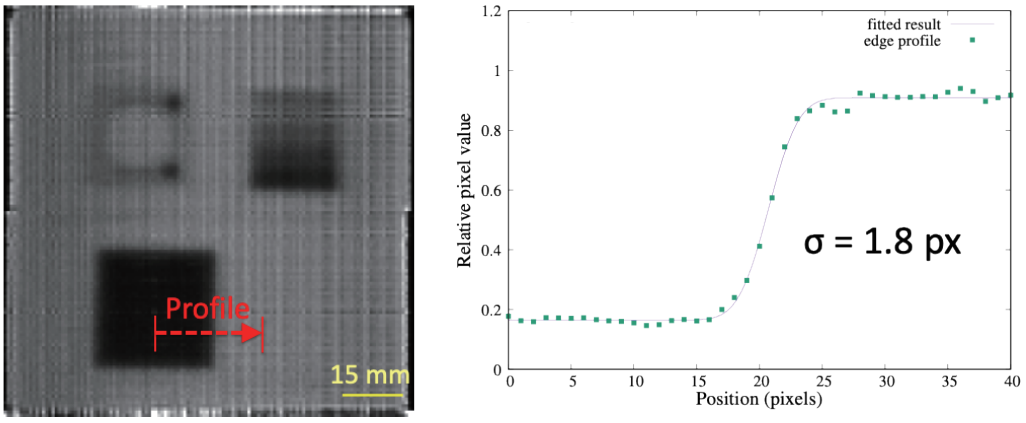

(a) (b)

Fig. 4. (Color online) (a) Neutron transmission image of a Cd plate (3 × 3 cm^2) and ASTM neutron indicators, acquired with a glass GEM detector with a total integration time of 116 min. The image is calibrated through X-strip direction. The red line in the figure indicates the area used to evaluate the spatial resolution. (b) Profile of the edges of the Cd plate and the results of fitting with an edge function to evaluate the spatial resolution.

From the result, the typical spatial resolution σ is 1.8 pixels, and since one pixel is 0.8 mm, the spatial resolution of the detector is evaluated as 3.3 mm (FWHM). This imaging result shows that all the components of the detector, including the neutron converter (boron cathode), glass GEM, readout strips, and data acquisition system, work properly. Figure 5(a) shows a typical neutron TOF spectrum obtained with this detector, which was placed at a distance of 8 m from the neutron source. The detection efficiency was evaluated by comparing the counting rate with that of a scintillation detector using a 1-mm-thick Li-glass scintillator. Figure 5(b) shows the ratio of the neutron detection count rate between the glass GEM detector and the Li-glass scintillation detector. By comparing the obtained values, the detection efficiency of the glass GEM detector was estimated to be 5% since the detection efficiency of the 1-mm-thick Li scintillator for 4 Å neutrons is almost 100%.[24]

Finally, we tested the ability of our detector to perform Bragg edge analysis using two steel samples: a 10-mm-thick body-centered cubic (bcc) steel plate and a 10-mm-thick face-centered cubic (fcc) steel plate. The obtained neutron transmission spectra are shown in

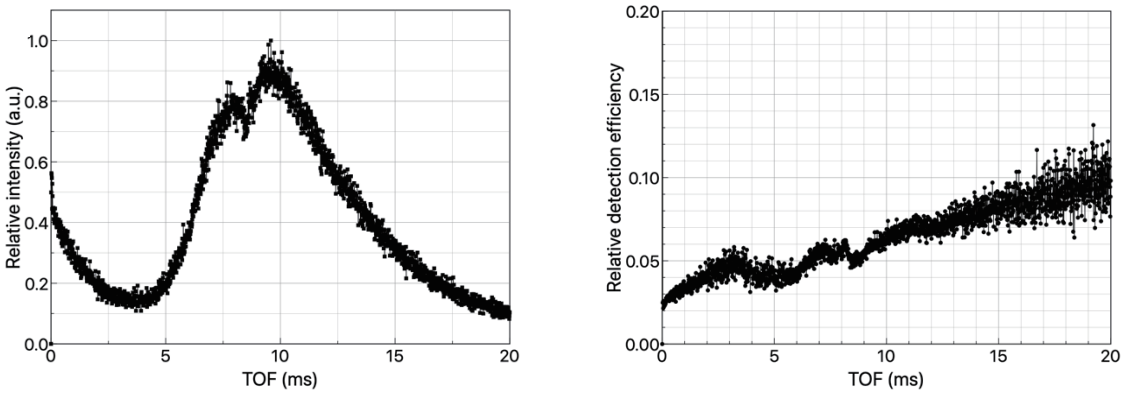

Fig. 5. (a) Typical neutron TOF. (b) Detection efficiency evaluation by comparison with Li-glass scintillation detector. The detection efficiency is estimated as 5% for 4 Å neutrons (≈TOF 8 ms).

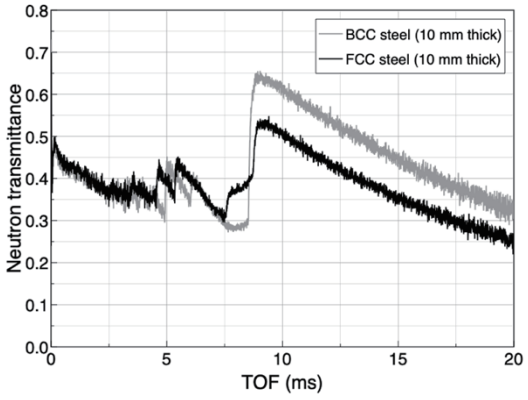

Fig. 6. Neutron Bragg edge spectra of bcc and fcc steel plates. A clear difference in the appearance of the Bragg edges was observed in the two steel samples.

Fig. 6, and it was confirmed that the Bragg edges had clearly different appearances in the bcc and fcc steel plates.

4. Conclusions

For Bragg edge neutron transmission imaging, we developed a time-resolved and position-sensitive detector with a micro-structured boron cathode, a glass GEM, and an X-Y strip readout system. Imaging experiments were conducted with this detector at AISTANS, and its basic performance was evaluated. The detector worked as expected and showed a high stability through the entire set of measurements. The obtained Bragg edge neutron transmission analysis results for bcc and fcc samples demonstrated the good energy/wavelength-selective neutron imaging ability of the detector. The neutron detection efficiency of the detector was evaluated as 5%, which we expect to increase by improving the process of fabricating the micro-structured boron cathode.

Acknowledgments

This paper is based on the results obtained from the JPNP14014 project commissioned by the New Energy and Industrial Technology Development Organization (NEDO).

References

1 B. Buras, K. Mikke, B. Lebech, and J. Leciejewicz: Phys. Status Solidi B **11** (1965) 567.
2 M. Kimura, M. Sugawara, M. Oyamada, Y. Yamada, S. Tomiyoshi, T. Suzuki, N. Watanabe, and S. Takeda: Nucl. Instrum. and Meth. **71** (1969) 102.
3 T. A. Gabriel, J. R. Haines, and T. J. McManamy: J. Nucl. Mat. **318** (2003) 1.
4 J. W. G. Thomason: Nucl. Instrum. Meth. **917** (2019) 61.
5 M. Arai and F. Maekawa: Nucl. Phys, News. **19** (2009) 34.
6 T. Shinohara, T. Kai, K. Oikawa, T. Nakatani, M. Segawa, K. Hiroi, Y. Su, M. Ooi, M. Harada, H. Iikura, H. Hayashida, J. D. Parker, Y. Matsumoto, T. Kamiyama, H. Sato, and Y. Kiyanagi: Rev. Sci. Instr. **91** (2020) 043302.
7 M. Furusaka, H. Sato, T. Kamiyama, M. Ohnuma, and Y. Kiyanagi: Phys. Procedia. **60** (2014) 167.
8 Y. Otake: Applications of Laser-Driven Particle Acceleration (CRC Press, Boca Raton, 2018) Chap. 19.
9 M. B. Leuschner, D. V. Baxter, V. P. Derunchuk, H. Kaiser, C. M. Lavelle, H. Nann, N. B. Remmes, T. Rinckel, W. M. Snow, and P. E. Sokol: Nucl. Instrum. Methods Phys. Res., Sect. A **261** (2007) 956.
10 K. Kino, T. Fujiwara, M. Furusaka, N. Hayashizaki, R. Kuroda, K. Michishio, T. Muroga, H. Ogawa, B. E.O'Rourke, N. Oshima, D. Satoh, N. Sei, T. Shishido, R. Suzuki, M. Tanaka, H. Toyokawa, and A. Watazu: Nucl. Instrum. Methods Phys. Res., Sect. A **927** (2019) 407.
11 K. Kino, M. Furusaka, T. Fujiwara, B. E.O'Rourke, T. Muroga, Yo Tomota, N. Oshima: Eur. Phys. J. Plus **137** (2022) 1260.
12 S. Uno, T. Uchida, M. Sekimoto, T. Murakami, K. Miyama, M. Shoji, E. Nakano, T.Koike, K. Morita, H. Satoh, T.Kamiyama, and Y. Kiyanagi: Phys. Procedia **26** (2012) 142.
13 J.D. Parker, M. Harada, K. Hattori, S. Iwaki, S. Kabuki, Y. Kishimoto, H. Kubo, S. Kurosawa, Y. Matsuoka, K. Miuchi, T. Mizumoto, H. Nishimura, T. Oku, T. Sawano, T. Shinohara, J. Suzuki, A. Takada, T. Tanimori, and K. Ueno: Nucl. Instrum. Methods Phys. Res., Sect. A **726** (2013) 155.
14 J. D. Parker, M. Harada, H. Hayashida, K. Hiroi, T. Kai, Y. Matsumoto, T. Nakatani, K. Oikawa, M. Segawa, T. Shinohara, Y. Su, A. Takada, T. Takemura, T. Taniguchi, T. Tanimori, and Y. Kiyanagi: Proc. 2016 IEEE Nucl. Sci. Symp. (NSS/MIC/RTSD) (2016) 1.
15 S. Satoh: JPS Conf. Proc. (2015) 051001.
16 N. Kawaguchi, D. Nakauchi, T. Kato, Y.Futami, and T. Yanagida: Sens. Mater. **34** (2021) 725.

17 K. Watanabe, T. Minniti, W. Kockelmann, R. Dalgliesh, G. Burca, A. S. Tremsin, Nucl. Instrum. Methods Phys. Res., Sect. A **861** (2017) p.55
18 F. Sauli: Nucl. Instrum. Methods Phys. Res., Sect. A **386** (1997) 531.
19 H. Takahashi, Y. Mitsuya, T. Fujiwara, and T. Fushie: Nucl. Instrum. Methods Phys. Res., Sect. A **724** (2013) 1.
20 T. Fujiwara, Y. Mitsuya, H. Takahashi, T. Fushie, S. Kishimito, B. Guerard, and M. Uesaka: J. Inst. **9** (2014) 11007.
21 T. Fujiwara, U. Bautista, Y. Mitsuya, H. Takahashi, N. L. Yamada, Y. Otake, A. Taketani, M. Uesaka, and H. Toyokawa: Nucl. Instrum. Methods Phys. Res., Sect. A **838** (2016) 124.
22 ASTM E2003-20, Standard Practice for Fabrication of the Neutron Radiographic Beam Purity Indicators (ASTM International, West Conshohocken, PA) (2020).
23 T. Fujiwara, Y. Mitsuya, T. Fushie, K. Murata, A. Kawamura, A. Koishikawa, H. Toyokawa, and H. Takahashi: Nucl. Instrum. Methods Phys. Res., Sect. A **850** (2017) 7.
24 K. Zhou, J. Zhou, Y. Song, X. Zhou, Z. Xie, G. Yang, Y. Wang, Y. Chen, and Z. Sun: Nucl. Sci. Tech **29** (2018) 127.